JPE 17-6-16

https://doi.org/10.6113/JPE.2017.17.6.1553
ISSN(Print): 1598-2092 / ISSN(Online): 2093-4718

# A Novel Control Scheme Based on the Synchronous Frame for APF

Yifan Wang*, Hong Zheng†,**, Ruoyin Wang*, and Wen Zhu*

†,*School of Electrical and Information Engineering, Jiangsu University, Zhenjiang, China
**Key Laboratory of Electric Vehicle Drive and Intelligent Control, Jiangsu University, Zhenjiang, China

## Abstract

For the purpose of enhancing the performance of the shunt active power filter (APF), this paper presents a novel Fast Weighted Compound Control (FWCC) strategy based on the synchronous frame. In this control strategy, the proposed new repetitive controller can work faster and more stably by reducing the internal model cycle and introducing a damping coefficient. In addition, the harmonic detector can be removed to simplify the structure of the APF owing to the improvements. Furthermore, a proportional-integral (PI) controller is added to work in parallel with the repetitive controller by using a weighted ratio. Then, a convergence speed analysis and design algorithm are given in detail. Simulation and experimental results show that the harmonic distortion is reduced from 2.91% to 1.89%. In addition, the content for each of the characteristic harmonic orders has decreased by more than three times.

**Key words:** Active power filter, Fast repetitive control, Internal model optimization, Harmonic compensation

## I. INTRODUCTION

In industrial production, numerous nonlinear power electronic devices have introduced a large amount of harmonics into the power grid, which can lead to power loss, voltage fluctuation, temperature rises of transformers, malfunctions of electronic equipment, etc. [1].

For the purpose of eliminating harmful harmonics in the grid, active power filters (APFs) that can compensate the harmonic currents generated by various kinds of devices and provide a fast response to load variations, are widely used [2], [3]. Normally, the performance of an APF is mainly influenced by its control strategy which depends most on the controller [4], [5]. How to design a controller with excellent dynamic and static performances is a hot issue in APF research [6], [7]. The conventional PI control, as a simple and effective control method, is widely used in APF current controllers. However, in practical applications, the harmonic current reference always contains harmonic currents of different frequencies, and the PI regulator cannot meet this requirement because of its bandwidth limitation [8]. Repetitive control, which is based on the internal model principle, can track the periodic reference signals or suppress the periodic disturbance signals in a closed-loop completely [9]-[13]. The repetitive controller successfully solves the problem of periodic signal tracking and disturbance elimination. However, the nature of the hysteresis of cycle control leads to a poor dynamic performance of the control system [14]. In order to improve the dynamic performance of a repetitive controller, a series of improved methods such as inner current loop control [15], [16] and state feedback control [17] are presented. A repetitive control strategy based on the synchronous coordinate system is proposed to improve the efficiency of the control scheme [18], [19]. In addition, a fast repetitive control with an optimized internal model is proposed in [20] to shorten the repetitive cycle. These control schemes can ensure a high quality sine wave of the grid current and guarantee a good dynamic performance of the control system. However, these strategies need too many control signals, which greatly increases the cost and volume of the system. This makes these algorithms hard to be applied in practical applications.

In power systems, there exists a certain type of harmonic current, which is generated by a six-pulse rectifier. Most of these harmonics are $6m\pm1$. According to the characteristics of this type of harmonics in the synchronous frame, a novel

Manuscript received Feb. 8, 2017; accepted Jul. 13, 2017
Recommended for publication by Associate Editor Young-Doo Yoon.
†Corresponding Author: Zhenghong0511@sina.com
Tel: + 86-511-88780035, Jiangsu University
*School of Electrical and Information Eng., Jiangsu University, China
**Key Laboratory of Electric Vehicle Drive and Intelligent Control, Jiangsu University, China

FWCC strategy that is based on the synchronous coordinate system, is presented. The proposed control scheme is composed of two main improvements. These improvements are a fast repetitive controller based on an optimized internal model and a weight coefficient in a compound control scheme.

First, a rapid repetitive controller is proposed. In this improved repetitive controller, it can be found that the internal model is significantly optimized. The repetitive period is only one sixth that of a traditional controller. This means that the response time of the controller becomes shorter and the control speed performance of repetitive controller is greatly improved. In addition, due to the optimization of the repetitive controller, the current signals collected from grid can be directly processed. In addition, by collecting the current signal directly from the grid, the structure of the APF is significantly simplified. Because the proposed repetitive controller can directly deal with the current signal from the grid after a coordinate conversion, the APF does not need a harmonic detection. In this way, the compensation performance of the APF is more accurate, since the control performance is no longer affected by the harmonic tracking process. However, although the performance of the repetitive controller is improved by using an optimized internal model, there is still a delay in the repetitive controller due to a drawback in the internal model principle.

Therefore, in order to overcome the limitation of a single control scheme, this paper designs a compound controller that is composed of an improved repetitive control and a PI control. Through the adjustment of a weighted coefficient, the control performance of the PI controller is enhanced, which gives the compound controller an excellent dynamic performance while the load is changing. In addition, the fast convergence performance of the proposed control scheme is analyzed in the middle of this paper. In order to enhance the robustness of the proposed control strategy, a damping coefficient $K_d$ is introduced in the internal model. By introducing this coefficient, the stable range of the control system is further expanded. This means that the APF system has a more stable margin in applications. Comparisons between the traditional and the improved strategy highlight the outstanding performance of the proposed control scheme. The design process of the controller parameters are given in detail. The feasibility and validity of the proposed control strategy are verified by simulation and experimental results.

## II. Analysis of the Improved Control Strategy

### A. Presentation of the FWCC Strategy

Fig. 1 shows the structure of a three-phase shunt APF system with an LCL output filter. The load in this paper is a nonlinear device which is usually a three-phase rectifier, which is often used as the front-ends of industrial AC drives. A shunt APF is

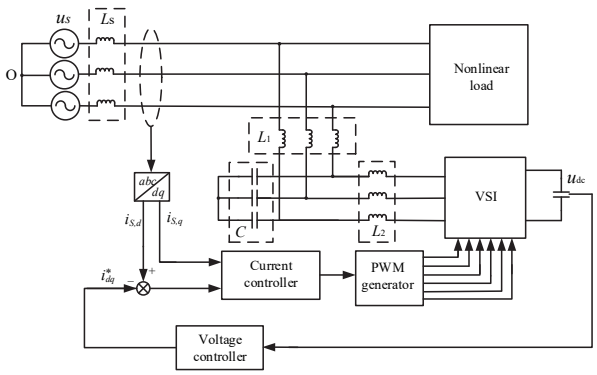


Fig. 1. Structure and control block of an APF system.

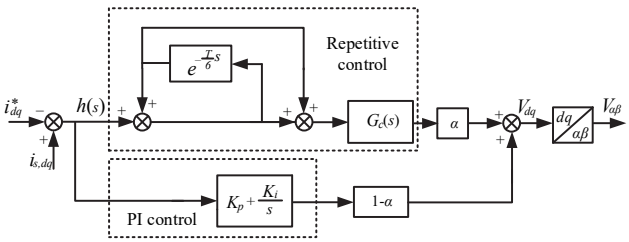


Fig. 2. The proposed FWCC strategy.

used as a source of the harmonic compensation, which can generate inverse harmonic current to eliminate harmonics in the grid.

In this paper, the main circuit of the APF is a three-phase voltage source inverter (VSI) connected in parallel with the load. The grid is connected to the APF through a LCL output filter, where $u_s$ is the voltage of the grid; $L_s$ is the inner inductance of the power supply; $u_{dc}$ is the DC capacitor of the VSI; and $L_1$, $C$ and $L_2$ are the parameters of the LCL output filter. The simplified APF control system is shown in Fig. 1, which consists of a voltage loop and a current loop. A PI controller is often used in the outer voltage loop to maintain a stable DC voltage of the APF. In addition, the inner current loop often uses a compound control to regulate the grid current and voltage in the same phase [21].

The proposed FWCC is shown in Fig. 2. It can be seen that the proposed scheme is composed of two main parts, which are the new improved repetitive control and the weight adjustment in a compound controller. It can be seen in Fig. 2 that the repetitive controller is improved through optimizing the internal model, which makes the repetitive control eliminate errors in grid faster. First, the supply current is transformed into the synchronous coordinate system and the current signal, which contains no fundamental component, is sent to compound controller. Then the proposed repetitive controller is executed to regulate the real current $i_{s,dq}$ to follow its reference $i^*_{dq}$ with the help of the PI control. For the purpose of improving the performance of the APF, while changing the load, a weight coefficient is introduced. As can be seen, the coefficient $a$ and 1-$a$ are added to the compound controller. Through this, the control effect of the parallel PI is

dramatically enhanced, and the APF has excellent switch performance between the static and dynamic conditions.

### *B. Fast Repetitive Control Based on an Optimized Internal Model*

In general, nonlinear loads generate numerous odd harmonics, which cause more damage than even harmonics. The increasing penetration of these odd harmonics has already deteriorated the power quality.

In industrial applications, considering a typical three-phase rectifier with a resistance-inductance load, most of the harmonics generated by a nonlinear load are $6m\pm1$ with $m$=1,2,3... [18]. Here, two phases of the three-phase grid are randomly selected to calculate the load currents. Phase a and phase b are taken as examples in this paper. The equations are given as:

$$\begin{bmatrix} i_a(t) \\ \\ i_b(t) \end{bmatrix} = \begin{bmatrix} \sum\limits_{\substack{n=6k+1 \\ k=1,2,3...}} (-1)^k I_n \cos(n\omega t) + I_1 \cos(\omega t) \\ \sum\limits_{\substack{n=6k+1 \\ k=1,2,3...}} (-1)^k I_n \cos\left(n\omega(t-\frac{2\pi}{3})\right) \\ + I_1 \cos\left(n\omega(t-\frac{2\pi}{3})\right) \end{bmatrix} \tag{1}$$

where $I_1$ is the fundamental current amplitude; $I_n$ is the $n$th current amplitude; $n$ is the harmonic order; $\omega$ is the fundamental angular frequency; and $k$ is a positive integer.

$$\begin{bmatrix} i_\alpha \\ i_\beta \end{bmatrix} = \begin{bmatrix} i_a \\ \dfrac{i_a + 2i_b}{\sqrt{3}} \end{bmatrix} \tag{2}$$

$$\begin{bmatrix} i_d \\ i_q \end{bmatrix} = \begin{bmatrix} i_\alpha \cos\omega t + i_\beta \sin\omega t \\ i_\beta \cos\omega t - i_\alpha \sin\omega t \end{bmatrix} \tag{3}$$

The equation of the current in the synchronous coordinate system is given as (4) by using transformation (3).

$$\begin{bmatrix} i_d(t) \\ \\ i_q(t) \end{bmatrix} = \begin{bmatrix} \sum\limits_{\substack{n=6k+1 \\ k=1,2,3...}} (-1)^k I_n \cos(n\omega t) + I_1 \\ \sum\limits_{\substack{n=6k+1 \\ k=1,2,3...}} (-1)^k I_n \cos\left(n\omega(t-\frac{2\pi}{3})\right) \\ + I_1 \cos\left(n\omega(t-\frac{2\pi}{3})\right) \end{bmatrix} \tag{4}$$

The load current spectrum of a typical three-phase rectifier is given in Fig. 3. It is found that the load current in the three phase frame only has $6m\pm1$ harmonics. Then, after the synchronous transformation, it can be seen that in addition to the DC component, there are only $6m$ harmonic currents left in the $dq$ coordinate system.

According to the characteristics of a typical load current in the $dq$ system, an improved repetitive control scheme is proposed. A block diagram of the traditional and improved repetitive internal models are shown in Fig. 4. It can be seen that the improved repetitive cycle is only one-sixth the traditional one. This means that the control speed can be greatly improved.

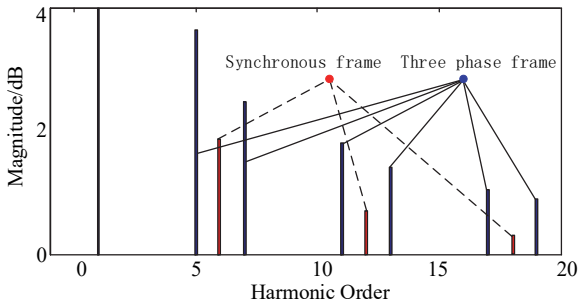


Fig. 3. Spectrum of the characteristic current.

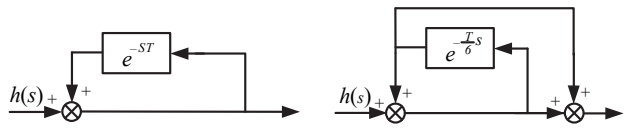


(a) Traditional internal model. (b) Improved internal model.

Fig. 4. Block diagram of the compound controller.

In addition, in this compound control strategy, the PI controller can achieve a rapid response to reference signal fluctuations, while the repetitive control can accurately track the output current. The transfer function of the repetitive controller is given as (5), and the function in the frequency domain can be modified as (6) by make $s=j\omega$.

$$G_R(s) = \frac{1+e^{-sT/6}}{1-e^{-sT/6}} \tag{5}$$

$$G_R(j\omega) = \frac{1+e^{-j\omega T/6}}{1-e^{-j\omega T/6}} \tag{6}$$

In the repetitive control, the period delay caused by the internal model controller has a great effect on the APF system response. This can directly affect the dynamic performance of the repetitive controller, which leads to an unsatisfactory tracking performance of the APF. The new internal model controller, whose repetitive period is only one-sixth of the conventional controller, is presented in (5). By optimizing the internal model, the repetitive control can have a more rapid response. In the above equations, $T=2\pi\omega_0$ and $\omega_0=2\pi f_0$ is the fundamental angular frequency.

Considering the characteristic of a typical three-phase rectifier, set $\omega=6m\omega_0$ ($m$=1, 2, 3...). Then by using the Euler formula, the transfer function of the repetitive controller can be modified as:

$$G_R(m) = \frac{1+\cos 2m\pi}{1-\cos 2m\pi} \tag{7}$$

It can be seen from (7) that this controller has infinite gains with $m$=1, 2, 3.... This means that the harmonic currents in the $6m\pm1$order, which act as $6i$ in the coordinate system, can

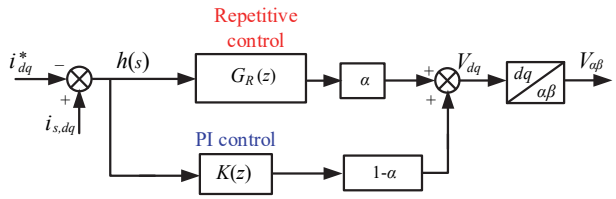

Fig. 5. Simplified FWCC block diagram.

be completely eliminated through the introduction of the new control. In addition, this control strategy is easy to digitally implement because of its simple model.

### C. Analysis of the Weight Coefficient

A block diagram of the FWCC method is shown in Fig. 2. From the discrete expressions of the tracking performance and anti-jamming performance shown in (8), where $G_R(z)$ is the expression of the repetitive control, it can be found that the performance of the system can be optimized through the rational design of the repetitive and PI control. The dynamic performance mostly depends on the PI control during fluctuations of the loads. However, the steady state performance (including the steady-state accuracy) and THD (Total Harmonic Distortion) of the system are determined by the repetitive control when the traditional compound controller reaches the steady state. The PI controller does not have a great regulation of the performance of the system when the load changes suddenly. This may result in a significant overshoot and a longer adjust time. Therefore, a single repetitive control cannot make the system achieve the best tracking performance and anti-jamming performance, which are usually mutually constrained. In order to improve the dynamic performance of the APF, a proportional coefficient $a$ is introduced to adjust the control weights of the repetitive control and PI control. A block diagram is shown in Fig. 5.

$$h(z)=\frac{I_L(z)-I_d(z)}{1+\alpha G_R(z)G_c(z)G_F(z)+(1-\alpha)G_F(z)K(z)} \tag{8}$$

The output of the RC branch or PI branch of the FWCC is different from that of the traditional method in the steady state. The introduction of the weighting factor enhances the performance of the PI control while switching the loads. It can be seen from (8) that although the FWCC affects the performance of the repetitive control in the steady state to some extent and leads to a small rise in the THD, the total performance of the APF can still be excellent. Due to the optimization of the fast repetitive control system, which simplifies the structure of the system and accelerates the response speed of the compound controller, it is possible to make up for the drawback of the coefficient introduction.

## III. Performance Analysis of the Improved Control Strategy

### A. Fast Convergence Speed

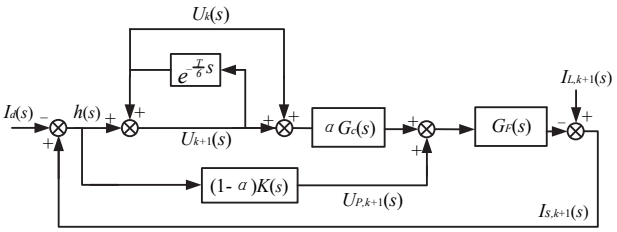

Fig. 6. Block diagram of the closed loop.

In order to analyze the convergence performance of the APF, a closed-loop control system is established in Fig. 6, where $K(s)$ is the transfer function of the PI controller, $G_c(s)$ is the compensation part of the repetitive controller, $G_F(s)$ is the transfer function of the LCL output filter, $I_s$(s) is the grid side current without a direct component, and $I_L$(s) is the load side current.

An analysis of the performance of the proposed control in the discrete-time domain is developed here, where $k$ is the repetitive cycle. The dynamic response time is set to $T/6$, where $T$ is the period of the traditional repetitive control.

Three equations can be obtained from Fig. 5 as (9), from which the current in last period of the supply side is given as (10).

$$\begin{cases} U_{k+1}(s)=U_k(s)+I_{s,k+1}(s)-I_d(s) \\ U_{P,k+1}(s)=(1-\alpha)K(s)[I_{s,k+1}(s)-I_d(s)] \\ I_{s,k+1}(s)=I_{L,k+1}(s)-U_{P,k+1}(s)G_F(s) \\ \qquad -\alpha G_c(s)G_F(s)[U_{k+1}(s)+U_k(s)] \end{cases} \tag{9}$$

$$\begin{aligned} I_{s,k}(s)=&I_{L,k}(s)+U_{P,k}(s)G_F(s) \\ &-\alpha G_c(s)G_F(s)[U_k(s)+U_{k-1}(s)] \end{aligned} \tag{10}$$

It is assumed that the APF system works in the steady state. Therefore, the current of the load side remains unchanged during two adjacent periods:

$$I_{L,k}(s)=I_{L,k+1}(s) \tag{11}$$

In sum of the results above, the following relationship holds:

$$\begin{aligned} I_{s,k}(s)-I_{s,k+1}(s)=&[U_{p,k+1}(s)-U_{p,k}(s)]G_F(s) \\ &+\alpha G_c(s)G_F(s)[U_{k+1}(s)-U_{k-1}(s)] \end{aligned} \tag{12}$$

where it is possible to replace the voltage parameters $U_p(s)$ and $U(s)$ with $I_s(s)$. Then the ratio of grid current in two adjacent periods can be derived from (9) and (12) as:

$$\begin{aligned} \frac{h_{k+1}(s)}{h_k(s)}&=\frac{I_{s,k+1}(s)-I_d(s)}{I_{s,k}(s)-I_d(s)} \\ &=\frac{1+(1-\alpha)G_F(s)K(s)-\alpha G_c(s)G_F(s)}{1+(1-\alpha)G_F(s)K(s)+\alpha G_c(s)G_F(s)} \\ &=1-\frac{2\alpha G_c(s)G_F(s)}{1+(1-\alpha)G_F(s)K(s)+\alpha G_c(s)G_F(s)} \\ &=1-G_A(s) \end{aligned} \tag{13}$$

where $h_{k+1}(s)$ and $h_k(s)$ are the harmonic values of two adjacent cycles. The remainder of the ratio can be assumed to be $G_A(s)$. It can be obtained from (13) that the error finally

becomes zero when $||G_A(s)||<1$. In addition, the smaller the $||G_A(s)||$ is, the shorter convergence time becomes [14].

Similarly, the error ratio of the conventional repetitive controller is given as:

$$\begin{aligned}\frac{I'_{s,k+1}}{I'_{s,k}} &= \frac{1+(1-\alpha)G_F(s)K(s)-\alpha G_F(s)G_c(s)}{1+(1-\alpha)G_F(s)K(s)} \\ &= 1-\frac{\alpha G_F(s)G_c(s)}{1+(1-\alpha)G_F(s)K(s)} \\ &= 1-G_T\end{aligned} \tag{14}$$

The ratio of the error equations between the improved control strategy and the traditional one can be obtained as:

$$\left\|\frac{1-G_A}{1-G_T}\right\| = \left\|\frac{1+(1-\alpha)G_F(s)K(s)}{1+(1-\alpha)G_F(s)K(s)+\alpha G_F(s)G_c(s)}\right\| < 1 \tag{15}$$

It can be concluded from the above equations that the proposed control scheme has a faster convergence speed when compared to the traditional control. This means that the improved control strategy can make a more rapid response to the current mutation. Then the performance of the APF is significantly improved.

### *B. Stability of the Proposed Control Strategy*

Maintaining system stability is a prerequisite for any advanced control. Meanwhile, the control system should have a larger stability margin to ensure the stability and good performance of the control system when there are parameter fluctuations or disturbance in the system.

As shown in Fig. 7, a discrete control block diagram is established. From this, the transfer function of the repetitive control in the z domain can be obtained as:

$$\frac{U_0(z)}{h(z)} = \frac{1+Z^{-\frac{N}{6}}}{1-Z^{-\frac{N}{6}}}G_c(z) = G_R(z)G_c(z) \tag{16}$$

The supply side harmonic current can be expressed as:

$$\begin{aligned}h(z) &= I_s(z)-I_d(z) \\ &= I_L(z)-G_F(z)[U_0(z)+(1-\alpha)h(z)K(z)]-I_d(z)\end{aligned} \tag{17}$$

Then the expression of the grid harmonic current can be derived from (16) and (17) as:

$$\begin{aligned}h(z) &= \frac{I_L(z)-I_d(z)}{1+\alpha G_R(z)G_c(z)G_F(z)+(1-\alpha)G_F(z)K(z)} \\ &= \frac{I_L(z)-I_d(z)}{1+(1-\alpha)G_F(z)K(z)+\alpha G_c(z)G_F(z)\dfrac{1+z^{-\frac{N}{6}}}{1-z^{-\frac{N}{6}}}}\end{aligned} \tag{18}$$

From (18), the system characteristic equation can be obtained as:

$$\begin{aligned}&z^{-\frac{N}{6}}[1-\alpha G_F(z)G_c(z)+(1-\alpha)G_F(z)K(z)] \\ &\quad -[1+\alpha G_F(z)G_c(z)+(1-\alpha)G_F(z)K(z)]=0\end{aligned} \tag{19}$$

$$z^{\frac{N}{6}} = \frac{1-\alpha G_c(z)G_F(z)+(1-\alpha)G_F(z)K(z)}{1+\alpha G_c(z)G_F(z)+(1-\alpha)G_F(z)K(z)} \tag{20}$$

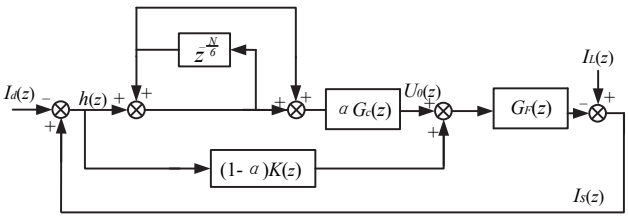


Fig. 7. Discrete diagram of the control system.

According to the definition of discrete system stability, the system is stable as long as all of the solutions of the characteristic equation are in a unit cycle. This is a necessary and sufficient condition for system stability. However, it is difficult to solve the high order equation. Therefore, the principle of small-gain theory is used here to solve this problem [22], [23]. A sufficient condition for system stability can be obtained as (21), which can be modified as (22).

$$\left|\frac{1-\alpha G_c(z)G_F(z)+(1-\alpha)G_F(z)K(z)}{1+\alpha G_c(z)G_F(z)+(1-\alpha)G_F(z)K(z)}\right| < 1 \tag{21}$$

$$\left|1-\frac{2\alpha G_c(z)}{\dfrac{1}{G_F(z)}+\alpha G_c(z)+(1-\alpha)K(z)}\right| = |1-G_x(z)| < 1 \tag{22}$$

It can be seen that (22) is always true when $G_F(z)\neq 0$. A vector diagram of this is shown in Fig. 7(c). However, in practical engineering, the system may become unstable due to the errors from modeling and phase compensation. In the medium and low frequencies, the phase and amplitude compensation errors are too small to affect the stability. Meanwhile, $G_x(z)$ is approximately equal to 1, which can satisfy (22). However, in high frequencies, $G_x(z)$ enters the second or fourth quadrant while phase compensation error is in the range of 90°-270°. This means that the solutions of (20) is out of the unit cycle, and the system is unstable.

For the purpose of ensuring the stability of the control system, the robustness of the proposed fast repetitive controller is analyzed. A damping factor $K_d$ is introduced in the internal model to improve the robustness of the control system. The improved internal model is shown in Fig. 8(b).

Then the sufficient condition of stability can be expressed as:

$$\begin{aligned}&\left|K_d-\frac{2\alpha G_c(z)G_F(z)}{1+\alpha G_c(z)G_F(z)+(1-\alpha)G_F(z)K(z)}\right| \\ &= |K_d-G_x(z)| < 1\end{aligned} \tag{23}$$

As can be seen in Fig. 8(d), the unit circle is tangent to the imaginary axis, and the system may become unstable. However, after the introduction of $K_d$, the stability range has a little shift to the left side. In addition, there is a small part of the unit circle in the second and fourth quadrant. If the factor $K_d$ is selected appropriately according to the range of $G_x(z)$ in this paper, the system must be stable. In this paper, due to the characteristic of a certain type of load, the output of the

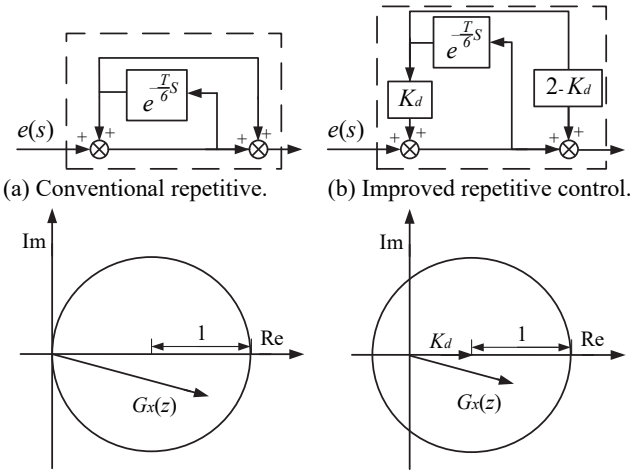


(a) Conventional repetitive. (b) Improved repetitive control.

(c) Conventional control vector. (d) Improved control vector.

Fig. 8. Vector diagrams and internal model block diagrams.

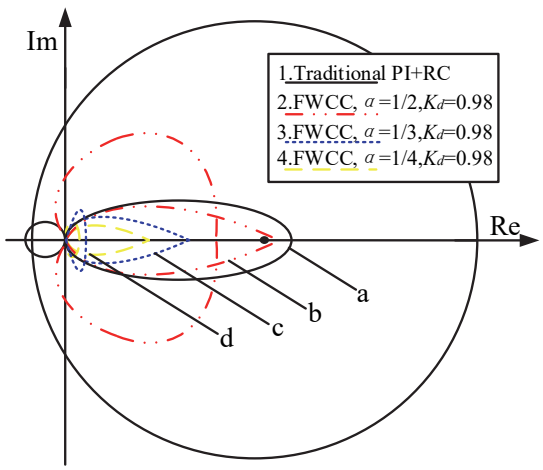


Fig. 9. Nyquist diagrams of different controls.

inverter contains few high-frequency harmonic orders. Therefore, the feed-back coefficient $K_d$ is set to 0.98 to meet the system stability requirements.

A Nyquist curve of system is shown in Fig. 9, where the system is stable if the trajectory is in the unit circle. In this figure, curve 1 is the trajectory of the traditional repetitive with a PI control. It can be seen that the system becomes unstable while in a high frequency. Curve 2 shows that the effectiveness of the FWCC method with $a$=1/2. It can be seen that the high frequency trajectory of the proposed strategy is smaller and that the system becomes stable. In addition, curve 3 and curve 4 have a smaller high frequency trajectory when compared with curve 1. This means that with the increasing of $a$, the system has a larger stable margin. In addition, this also indicates the poor regulation performance of the PI control in the traditional compound control strategy, while the system is working in the steady state. However, by using the FWCC scheme and adjusting the weighting coefficient, the control performance of the PI controller is significantly enhanced. This directly enhances the robustness of system and improves the conversion performance between the dynamic state and the static state.

## IV. Parameter Design

Although the PI controller cannot achieve zero-error tracking for the bandwidth limitation, its fast response performance to load fluctuations can make up for the inadequacy of the repetitive control [24].

When designing the proportion parameter of the PI controller, it is necessary to ensure a great open-loop bandwidth for compensating the highest harmonic frequency. Additionally, in the digital control system, the output of the controller usually delays about one switching period due to the influence of the system sampling and computing time. In order to ensure a large enough phase margin for the PI controller to maintain the stability of the closed-loop system, the open-loop gain $k_p$ should not be too large. Moreover, due to the discreteness of the digital system, there is still a certain amount of errors. Therefore, an overlarge $k_p$ leads to a loss of the control accuracy and makes the system unstable. In addition, a $k_p$ which is too small for the PI controller to regulate the current, may reduce the adjustment accuracy and make the response slow. This will further prolong the adjustment time and affect the dynamic and static performance of the system.

The integral coefficient $k_i$ is used to eliminate the static error of the system and to improve the accuracy of the APF. The controller easily overshoots, which is likely to make the system unstable if it is designed inappropriately. Based on the above considerations, $k_p$=15 and $k_i$=4.

The performance of the repetitive controller is dramatically influenced by its compensator $G_c(z)$. In this paper, the repetitive controller is improved through the optimization of the internal model. Therefore, it is possible to use the traditional methods to design the compensator for the improved controller.

In the design of the repetitive controller, $G_c(z)$ is composed of three main parts and is usually written as $k_rC_1(z)C_2(z)$, where $k_r$ is the gain coefficient regulating the gain of the repetitive loop, which can accelerate the error convergence rate of the repetitive control. $C_1(z)$ provides high frequency attenuation. In order to avoid an over-large high frequency gain, a low-pass second-order filter is used [25]. According to Fig. 1, the transfer function of the controlled object can be given as:

$$G_F(s)=\frac{L_1L_2Cs^2+L_1}{L_1^2L_2Cs^3+(L_1^2+L_1L_2)s} \tag{24}$$

As can be seen in (24), the function is a typical three-order system, and the phase shifting from the low frequency to the middle frequency is not obvious. Therefore, the common form of a low-pass second-order filter can be obtained as:

$$C_1(s)=\frac{\omega^2}{s^2+2\omega\mu s+\omega^2} \tag{25}$$

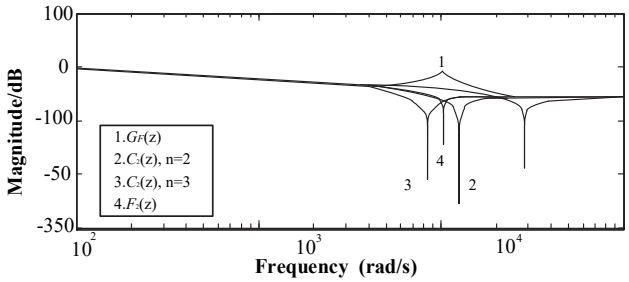


Fig. 10. Amplitude-frequency characteristics of the inverter and compensator.

$$C_2(z)=\frac{\sum_{r=1}^{m}\alpha_r z^{r}+\sum_{r=1}^{m}\alpha_r z^{-r}}{\alpha_0+2\sum_{r=1}^{m}\alpha_r} \tag{26}$$

Here, for the purpose of preventing resonance in the control loop and meeting the requirement of $\mu$>0.707, the coefficient is set to $\mu$=0.8. Under normal circumstances, a zero phase shift filter $C_2(z)$ is usually used to give the converter a negative gain to eliminate the resonant peak at the cut-off frequency. The zero phase shift filter makes the gain remain almost constant when the converter works in a frequency lower than the cut-off frequency, but the gain decays rapidly when the converter works in a frequency higher than the cut-off frequency [26]. The expression of the filter is taken as (26), where $\alpha_0$ and $\alpha_r$ are the weight coefficients. Considering that the controller becomes more complicate when the order of $C_2(z)$ is higher than three, and to give $k_r$ a wider stable range at the same time, n can be valued at 2 or 3. However, the generated notch and resonant frequency of the inverter are not completely matched, which means that the compensation performance is greatly affected. The compensation performance is shown in Fig. 10, where curve 2 and curve 3 show the amplitude-frequency diagram of the zero phase shift filter. In order to solve this problem, a characteristic frequency notch filter is used in this paper, and its general expression can be given as:

$$F_2(z)=q\frac{(z-e^{j\omega T_s})(z-e^{-j\omega T_s})}{(z-pe^{j\omega T_s})(z-pe^{-j\omega T_s})} \tag{27}$$

where $\omega$ is the notch frequency, $p$ is the opening coefficient, and $q$ is the gain coefficient of the notch filter. Here, ω is equal to the no-load resonant frequency, $p$=0.72 and $q$=0.8.

In addition, in order to compensate the phase delay caused by the controlled object and compensator, the coefficient $k$ is introduced into the repetitive controller. Then the delay from the PWM modulation and sampling process can be compensated. Here, the phase compensation coefficient is $k$=2.

As can be seen in Fig. 11, curve b is a bode of the transfer controlled object and curve a is a diagram after compensation. It can be found that curve b has two resonant peaks which makes the control system unstable. However, curve a is approximately a straight line, which means that the resonant humps are effectively restrained.

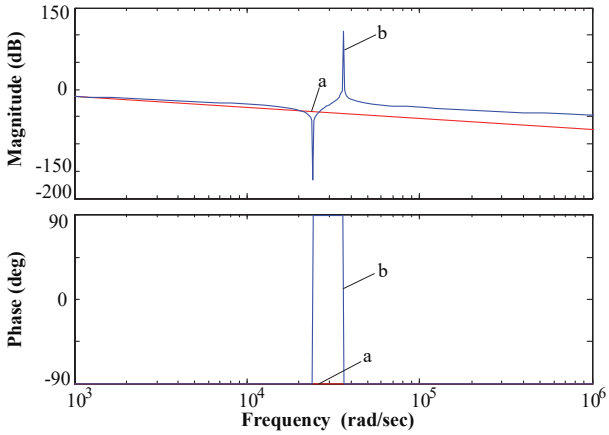


Fig. 11. Bode diagram of the compensation performance.

TABLE I
SIMULATION PARAMETERS

| | |
|---|---|
| $L_1$ | 1.5mH |
| $L_2$ | 8mH |
| $L_s$ | 2mH |
| $C$ | 8$\mu$F |
| Sampling frequency | 15kHz |
| Grid frequency | 50Hz |
| Phase voltage | 220V |
| Direct voltage | 400V |

## V. SIMULATION AND EXPERIMENTAL RESULTS

### *A. Simulation Verification*

In order to demonstrate the effectiveness of the proposed control algorithm, a simulation based on Matlab/Simulink is developed. An APF system is established according to Fig. 1, where a six-pulse rectifier bridge with a load of resistance and inductance is used as a source of harmonic. The detailed system parameters are shown in TABLE I.

Due to the delay of the internal model, the repetitive controller does not work until 0.02s. Therefore, the simulation results all begin at 0.02s. Fig. 12(a) shows the supply current with the introduction of the traditional repetitive control. It can be seen that the resonant peaks are suppressed from 0.02s and that they remain unchanged at around 0.09s. According to the FFT (Fast Fourier Transform), the THD (Total Harmonic Distortion) of the supply current after compensation is about 2.91%. It can be found in Fig. 12(b) that most of the harmonics are $6m\pm1$. However, the compensation performance of the proposed control algorithm is shown in Fig. 12(c). The resonant humps decrease to their minimum at 0.06s and remain stable in the

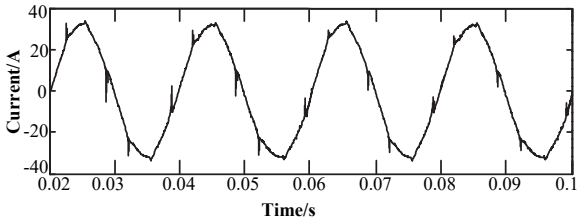


(a) Compensation performance of the traditional repetitive control.

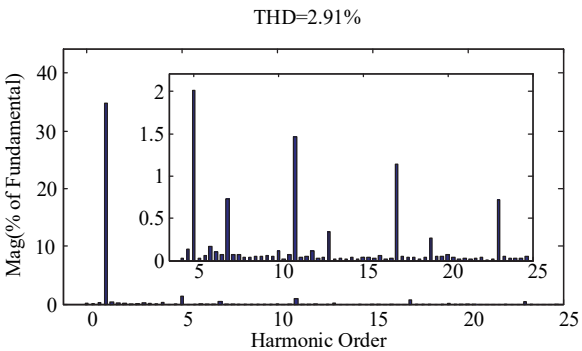


(b) FFT analysis of the traditional control.

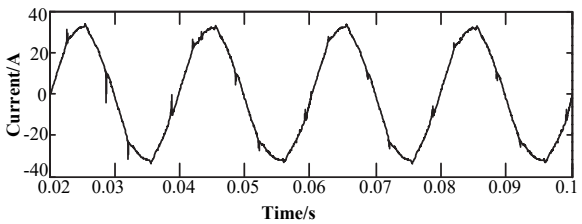


(c) Compensation performance of the proposed control scheme.

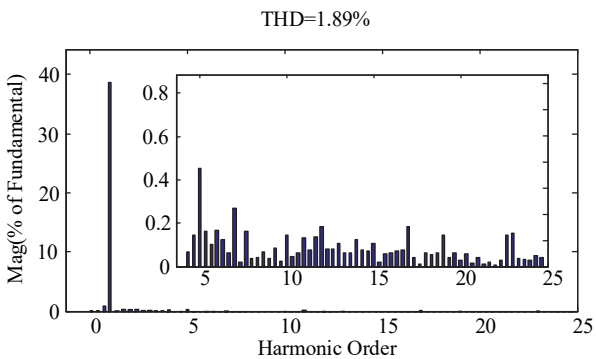


(d) FFT analysis of the improved control.

Fig. 12. Matlab simulation results.

last 0.04s. This indicates that the proposed control scheme can depress the resonance more rapidly and that the improved APF system has a smaller steady error. It can also be found that the THD is reduced to 1.89% and that the characteristic harmonics are eliminated by nearly half when compared to that of the traditional control.

### *B. Experimental Verification*

To verify the validity of the proposed controller, a three-phase parallel APF prototype is established as shown in Fig. 13.

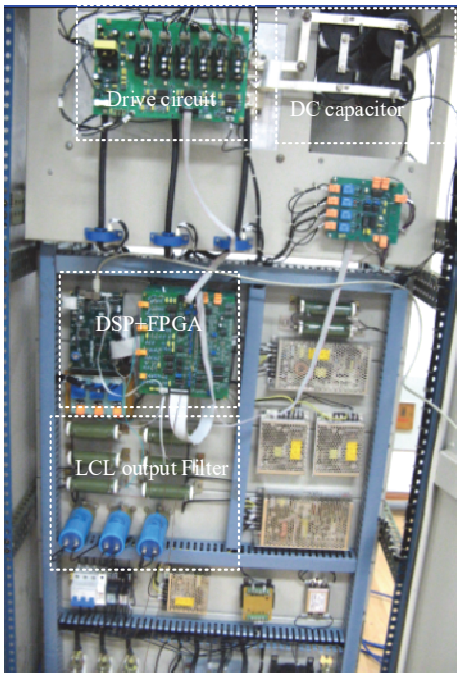


Fig. 13. Prototype of a shunt APF.

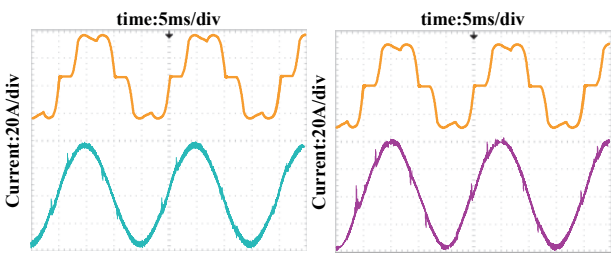


(a) Improved control. (b) Traditional control.

Fig. 14. Experimental results.

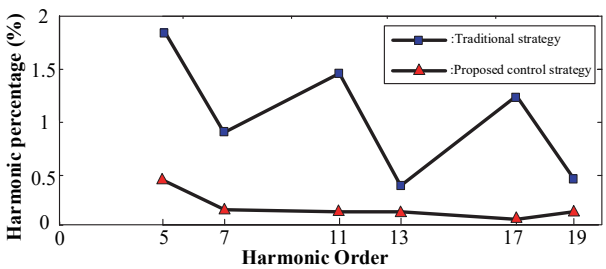


Fig. 15. Comparison of the harmonic contents.

The APF control system is based on a TMS320F2812 (150MHz/32bit) integrated into a SEED-DEC2812 EVM circuit board and a Cyclone III EP3C25 FPGA. The DSP is responsible for device protection, data analysis and human-computer interaction. The FPGA achieves the A-D sampling, repetitive control and PWM generation.

Fig. 14 shows experimental results of the traditional and proposed controls. It can be seen that the experimental results are consistent with those of the simulation, which verifies the validity of the proposed scheme. Fig. 15 gives a detailed comparison of the traditional and improved controls.

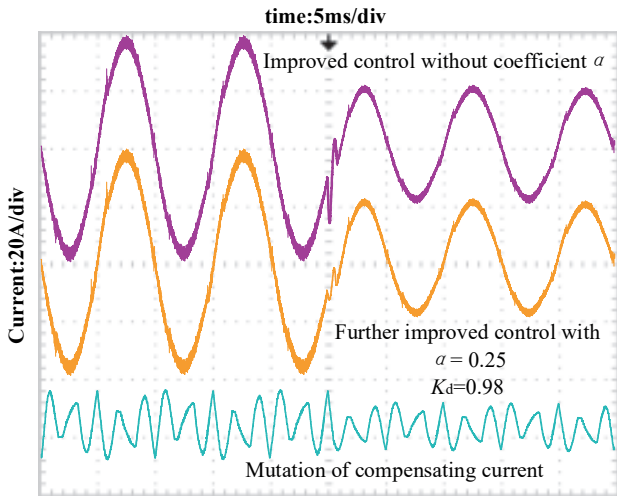

Fig. 16. Dynamic experimental results.

From the comparison it can be found that the characteristic harmonics are dramatically restrained. All of the $6m\pm1$ orders are attenuated by more than three times, which indicates the suppression performance of the proposed strategy for a certain type of harmonics in the power grid.

To verify the dynamic response performance of the APF system, the load is set to mutate while the APF is working in the steady-state. As shown in Fig. 16, the current is not dramatically affected when the load changes with the use of the weighted coefficient *a* when compared with the improved control method proposed in first part of this paper. In addition, the compensating current in Fig. 16 changes smoothly while the load changes. This verifies the good dynamic compensation performance of the APF system with the introduction of the coefficient *a*.

## VI. Conclusion

In this paper, an advanced current controller based on the synchronous reference frame was proposed. According to the control system block and convergence function, the static and dynamic performances of the APF system were analyzed. The convergence analysis verified the stability and the rapid response of the proposed compound control strategy. The working principle and system stability of the proposed control scheme were analyzed. After that, the design of the controller was given in detail. The theoretical analysis and simulation show that the proposed control strategy can improve the stability of the system and eliminate the $6m\pm1$ harmonics with fewer steady-state errors and a faster convergence speed when compared to the traditional control strategy. The good performance of the dynamic process is verified by the experimental results.

## Acknowledgment

This work is supported in part by the Project Funded by the Academic Program Development of Jiangsu Higher Education institutions (PAPD).

## References

[1] T. H. Ortmeye, K. R. Chakravarthi, and A. A. Mahmoud, "The effects of power system harmonics on power system equipment and loads," *IEEE Power Engineering Review*, Vol. PER-5, No. 9, pp.54, Sep. 1985.

[2] H. Akagi, "New trend in active filters for power conditioning," *IEEE Trans. Ind. Appl.*, Vol. 32, No. 6, pp. 1312-1332, Nov./Dec. 1996.

[3] H. Akagi, E. H. Watanabe, and M. Aredes, *Instantaneous Power Theory and Application to Power Conditioning*, M. E. El-Hawari, Ed. New York: Wiley, 2007.

[4] T. Ghennam, E. M. Berkouk, and B. Francois, "A novel space-vector current control base on circular hysteresis areas of a three-phase neutral-point-clamped inverter," *IEEE Trans. Ind. Electron.*, Vol. 57, No. 8, pp. 2669-2678, Aug. 2010.

[5] Q. Yang, J. Gao, Y. Zhao, and X. Guo, "Research on specific harmonic control strategy for active power filter," *Power System Protection and Control*, Vol. 40, No. 3, pp. 119-123, Mar. 2012.

[6] J. Zhou, J. Qin, Z. Wang, and X. Wu, "Application of deadbeat control with plug-in repetitive controller in active power filter," *Transactions of China Electrotechnical Society*, Vol. 28, No. 2, pp. 233-238, Feb. 2013.

[7] J. Yu, Z. Teng, J. Zhang, and K. Hu, "Predictive current control and stability analysis of active power filter," *Transactions of China Electrotechnical Society*, Vol. 24, No. 7, pp. 164-170, Jul. 2009.

[8] M. Rashed, C. Klumpner, and G. Asher, "Repetitive and resonant control for a single-phase grid-connected hybrid cascaded multilevel converter," *IEEE Trans. Power Electron.*, Vol. 28, No. 5, pp. 2224-2234, May 2013.

[9] C. Li, D. Zhang, and X. Zhuang, "Repetitive control-a survey," *Electric Machine and Control*, Vol. 9, No. 1, pp. 37-44, Jan. 2005.

[10] S. Hara, Y. Yamamoto, T. Omata, and M. Nakano, "Repetitive control systems: a new type servo system for periodic exogenous signals," *IEEE Trans. Autom. Control*, Vol. 33, No. 7, pp. 659-668, Jul. 1988.

[11] R. Costa-Castello, R. Grino, and E. Fossas, "Odd-harmonic digital repetitive control of a single-phase current active filter," *IEEE Trans. Power Electron.*, Vol. 19, No. 4, pp. 1060-1068, Jul. 2004.

[12] Z. Zou, Z. Wang, M. Cheng, and Y. Yang, "Active power filter for harmonic compensation using a digital dual-mode-structure repetitive control approach," in *3rd IEEE International Symposium on Power Electronics for Distributed Generation Systems (PEDG)*, pp. 161-166, Jun. 2012.

[13] P. Mattavelli and F. P. Marafao, "Repetitive-based control for selective harmonic compensation in active power filters," *IEEE Trans. Ind. Electron.*, Vol. 51, No. 5, pp. 1018-1024, Oct. 2004.

[14] K. Zhang, Y. Kang, J. Xiong, and J. Chen, "Direct repetitive control of SPWM inverter for UPS purpose," *IEEE Trans. Power Electron.*, Vol. 18, No. 3, pp. 784-792, May 2003.

[15] G. Teng, G. Xiao, Z. Zhang, Y. Qi, and Y. Lu, "A single-loop current control method for LCL-filtered grid-connected inverters based on the repetitive

controller," *Proceedings of the CSEE*, Vol. 33, No .24, pp. 13-21, Oct. 2013.
[16] Z. Qiu, E. Yang, J. Kong, and G. Chen, "Current loop control approach for LCL-based shunt power filter," *Proceedings of the CSEE*, Vol. 29, No. 18, pp. 15-20, Jun. 2009.
[17] Z. Huang, X. Zou, L. Tong, Y. Kang, and Q. Huang, "Research on current mode single-phase dynamic voltage regulator based on pole-assignment and repetitive control," *Transactions of China Electrotechnical Society*, Vol. 27, No. 6, pp. 252-260, Jun. 2012.
[18] B. F. Chen, X. M. Zha, J. W. Gong, S. X. Guo, and J. J. Juan, "Realization and improvement of repetitive control in synchronous frame for active power filter Power Electronics system," in *IEEE 25th Applied Exposition Conference and CA*, No. 2, pp. 21-25, Feb. 2010.
[19] J. Wu, N. He, and D. Xu, "Application of repetitive control technique in shunt active power filter," *Proceedings of the CSEE*, Vol. 28, No. 18, pp. 66-72, Jun. 2008.
[20] G. N. Trinh and H. H. Lee, "An advanced current control strategy for three-phase shunt active power filters," *IEEE Trans. Ind. Electron*., Vol. 60, No. 12, pp. 5400-5410, Dec. 2013.
[21] J. Gong, X. Zha, and B. Chen, "Analysis and realization of a fast repetitive controller in active power filter system," *Transactions of China Electrotechnical Society*, Vol. 26, No. 10, pp. 110-117, May 2011.
[22] F. Liu, J. Gong, G. Peng, P. Wang, and X. Zha, "Application of compound Repetitive Control in Shunt Active Power Filter," *Transactions of China Electrotechnical Society*, Vol. 27, No. 12, pp. 138-145, Dec. 2012.
[23] Z. Qiu, E. Yang, J. Kong, G. Chen, "Current loop control approach for LCL-based shunt active power filter," *Proceedings of the CSEE*, Vol. 29, No. 18, pp. 15-20, Jun. 2009.
[24] C. Wang, X. Zou, Y. Xu, Y. Zou, Y. Zhang, W. Chen, X. She, and F. Liu, "Improved repetitive control scheme for power electronic load," *Proceedings of the CSEE*, Vol. 29, No. 12, pp. 1-9, Apr. 2009.
[25] X. Zhang, Y. Wang C. Yu, C. Qi, and Y. W. Zhang, "Mechanism of the control coupling and suppression strategy using PI and repetitive control in grid-connected inverters," *Proceedings of the CSEE*, Vol. 34, No. 30, pp. 5287-5295, Nov. 2014.
[26] J. Yu, M. Su, and Y. Sun, "Improved repetitive control and its optimization for active power filter," *Transations of China Electrotechnical Society*, Vol. 27, No. 2, pp. 235-242, Feb. 2012.

**Yifan Wang** was born in China, in 1991. He received his B.S. degree from Jiangsu University, Zhenjiang, China, in 2015, where he is presently working toward his M.S. degree in Electrical Engineering. His current research interests include grid-connected inverters, power electronics and power quality control.

**Hong Zheng** was born in Anhui, China. He received his B.S. and Ph.D. degrees in Power Electronics and Drives Engineering from Jiangsu University, Zhenjiang, China, in 1987 and 2011, respectively. He worked as a Chief Engineer in the Xi'an Power Electronics Research Institute, Xi'an, China. Since 2009, he has been working as a Professor in the School of Electrical and Information Engineering Jiangsu University. His current research interests include power electronic converters, custom power technology and power quality control technology for smart grids, distributed generation and energy storage technology.

**Ruoyin Wang** was born in China, in 1991. He received his B.S. degree from the Jiangsu University of Science and Technology, Zhenjiang, China, in 2013. He is presently working toward his M.S. degree in Electrical Engineering from Jiangsu University, Zhenjiang, China. His current research interests include power electronics, photovoltaic inverters and electric drives.

**Wen Zhu** was born in China, in 1992. He received his B.S. degree from the Jingjiang College of Jiangsu University, Zhenjiang, China, in 2015. He is presently working toward his M.S. degree in Electrical Engineering from Jiangsu University, Zhenjiang, China. His current research interests include power electronics and AC-DC converters.